A Model for Stacked Rapid Sand Filters

Theresa Chu[⋆*], Jonathan Harris[*], Lucinda Li[*], and William Pennock[*]

[⋆]Corresponding Author
[*]220 Hollister Hall, Cornell University, Ithaca, NY 14853.

Abstract

Dynamic models of stacked rapid sand filtration has proved elusive in accounting for the diminishing pore space and increasing head loss. Empirical data has shown that head loss increases linearly over time despite filter breakthrough. Dirty filter bed head loss shows that minor losses add to head loss over time. A new model for dynamic filtration is proposed, which models captured particles as embedded rings of flocs in the filter bed. Particle removal through filtration is described with an active filtration zone of empty pores filling up with particles. This zone moves throughout the layer of sand until there is no available pore space and surface area for particles to attach.

Keywords: sand filters, dynamic modeling, water treatment

Introduction

Sand filtration has been used in drinking water treatment for particle removal for over a century, but a fuller understanding of the processes remains elusive. As stated by Benjamin and Lawler (2013), "if one believes that the purpose of modeling is to be able to predict *a priori* the full behavior of filters, then the modeling efforts to date have been been a failure."

A model to predict the full dynamic behavior of a stacked rapid sand (StaRS) filter has yet to be attempted. Unlike traditional rapid sand filters,

StaRS filters have multiple layers of uniform sand between alternating inlet pipes and outlet pipes. Each layer of sand acts as an independent filter where a portion of the flow is treated in each layer. As described by Adelman et al. (2012), water is injected in the sand, where half of the water flows upward and half flows downward. The water exits through outlet pipes at the top or the bottom of each layer. To better understand the behavior of a StaRS filter and characterize filter failure time, the performance parameters of effluent turbidity and head loss were measured.

In a typical filter run, effluent water quality and head loss determine the allowable time or cumulative volume throughput until backwashing is necessary. A period of ripening starts the filtration run when the filter bed is clean of particles and is filled with clean water. During ripening, effluent concentration decreases significantly until reaching a steady state value. This ripening process occurs because captured particles in the path of flow increase collisions and particle-particle interactions help improve future particle capture. If the filter run is long enough, the effluent concentration remains at a steady state value until breakthrough, where the effluent concentration increases because either influent particles can no longer attach or previously captured particles are breaking off from the filter. The filter run will end either when the effluent concentration begins to increase again and reaches the maximum allowable value or when the maximum allowable head loss is reached, whichever occurs first. The maximum allowable head loss is determined by considering physical and economic constraints such as the diameter and length of the filter, which determine the maximum storage capacity or the maximum pumping head available. Moreover, head loss increases linearly with the filter run time (Benjamin and Lawler, 2013).

Many models have been created to predict filter performance given filter and operational parameters. Jegatheesan and Vigneswaran (2003) state that modeling approaches to the filtration process can be categorized into two broad approaches: microscopic and macroscopic.

The macroscopic approach does not expressly account for the physical and chemical characteristics of filtration; instead they are accounted for by the filter coefficient, λ, the probability that a particle will be captured per unit length of the filter (Iwasaki et al., 1937). This coefficient is empirically determined from measurements from the specific system. Therefore every system will have a unique λ. There have been many attempts at a mathematical description of granular media filtration beginning in 1937 when Iwasaki et al.

found a first order differential equation with respect to depth:

$$\frac{\partial C}{\partial z} = -\lambda C. \tag{1}$$

Equation 1 described the partial derivative of the particle concentration, C, over the partial derivative of depth of the sand layer, z, as a function of the filter coefficient, λ, times concentration. This equation can then be integrated:

$$\int_{C_0}^{C} \frac{\partial C}{C} = -\lambda \int_{0}^{L} \partial z \tag{2}$$

and solved

$$\ln \frac{C}{C_0} = -\lambda L. \tag{3}$$

In Equation 3, experimental values of λ can be found, where L is the total depth of the media bed, C_0 is the concentration going into the filter and C is the concentration of particles exiting the filter.

A macroscopic model was created to depict a sand filter column in a study by Zhi (2016). In this study, Arsenic (V) was removed by adsorption onto PACl precipitates inside a sand filter column. As the precipitates accumulated in the filter column, head loss increased and the filter approached failure. Various coagulant dosages were employed in the study to examine the optimal coagulant dosage for As removal efficiency. When filter performance was examined during As removal, head loss increased with the cumulative mass of coagulant in the filter. These results suggest that different influent coagulant dosages did not alter the size of the coagulant precipitates. The head loss was modeled as a function of the cumulative mass of coagulant entering the filter.

In the microscopic approach, the removal of particles in a filter can be represented as performed by an aggregate of collectors (the media grains) that particles attach to, with a unique geometry that the fluid flows through. Some microscopic models include the spherical-in-cell model, isolated spherical model, capillaric model, and the constricted tube model. These models can only be used for initial particle deposition, and are not helpful when particles begin to clog the filter.

The spherical model defines the geometry of the media as tiny spheres with a diameter, d_g, which is the average diameter of the media grains(Zamani and Maini, 2009). The spherical-in-cell model was described by Rajagopalan

and Tien (1976) as a semi-empirical expression for filtration that relates collection efficiency to operating parameters. These parameters are the gravitational force, the attractive surface London forces, random forces that induce Brownian motion, and the ratio of media size to particle size. The isolated spherical model simplifies each particle grains as a sphere and assumes that each grain is not affected by the presence of the surrounding media grains (Rajagopalan and Tien, 1977).

The capillaric model defines the filter as a number, n of straight capillary tubes with equal radii a_c and lengths l. The length of each capillary section is assumed to be equal to the average media grain diameter. The porosity, ϵ, and the permeability, k , are given by the equations:

$$\epsilon = n\pi a_c^2 \tag{4}$$

and

$$k = \frac{\epsilon a_c^2}{8}. \tag{5}$$

Unlike the isolated spherical model, the constricted tube model takes into account the effects of surrounding grains. Also, unlike the capillary model, in this model the flow geometry created by spherical grains does not consist of tubes of a consistent diameter, but rather a series of constrictions and expansions. Each series is not necessarily of the same size in length or diameter. The constricted tube model suggests that the particle collection efficiency is dependent on the geometry of the media. The diameter of the expansions in the constricted tube is d_{max} and the diameter of the constrictions is d_c.

These models generally only apply with the filter is first clean and do not model dynamic filtration.

Mathematical Model

Capillary Model

For the study of dynamic filter performance, the pore storage space of the filter media was first modeled as many small capillary tubes within the larger column, much like the capillaric model, Figure 1. The visual representation of the capillary model is very similar to that of the previously mentioned capillaric model. However, the approaches taken in each model to calculate the diameter of each capillary were very different. In the capillary model,

each capillary tube has a height that is equal to the depth of a sand bed layer and a diameter that is equal to that of a pore as determined by the porosity-diameter relationship,

$$\eta = \frac{D_{\text{Cap}}^2}{D_{\text{Cap}}^2 + D_{\text{Sand}}^2}. \tag{6}$$

The capillary tubes are parallel to one another and form a bundle of capillary tubes within the filter such that the cross sectional cut of the filter consists of many circles that fill up the filter cross sectional area, as shown in Figure 1. This depiction of pore storage space allows for a few simplifications of the filtration model. It is common to assume laminar flow through the pore volume in a sand filter, and, correspondingly, flow through a capillary tube is also laminar. However, actual flow through the filter involves mixing and bending as the water weaves through the sand particles. Despite the discrepancy, an analysis of head loss through a clean bed filter detected only major head losses, further validating that flow through a capillary tube is laminar.

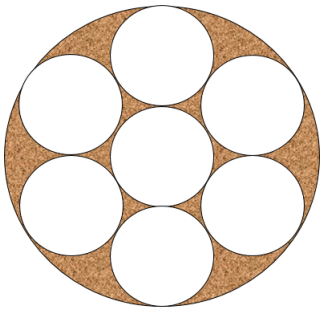

Figure 1: Shown is a zoomed-in plan view of the capillaries where the white circles represent capillaries.

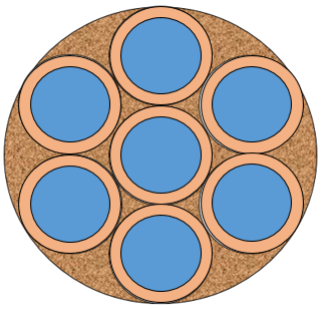

Figure 2: Shown is a zoomed-in plan view of one capillary tube. The outer, lighter-colored ring represents floc build-up on the sides and the blue regions are where water flows through the tube.

When flocs enter the filter, they are modeled as being captured within the capillary tubes, coating the sides of the media. The capillary reaches its maximum capacity when the diameter is small enough for the limiting shear to occur at the walls. Figure 2 demonstrates a clean capillary tube and a capillary tube at maximum capacity.

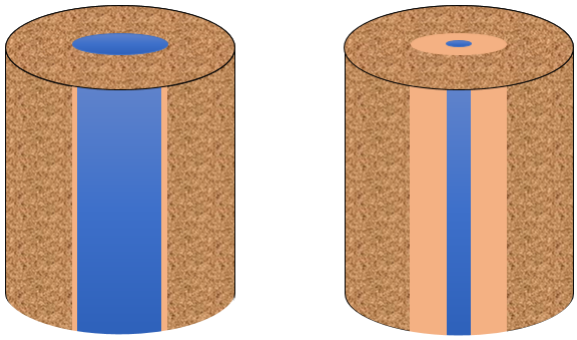

Figure 3: On the left hand side is an illustration of initial particle accumulation in one concentrated region and on the right hand side is an illustration of a capillary tube that is entirely filled with flocs.

However, further analysis of the model revealed a discrepancy between an empirically-calculated floc density and a theoretical range of possible floc densities, suggesting that the capillary model is not a realistic representation of filtration in the StaRS filters. In calculating the empirical floc density,

the diameter of a capillary during filter failure was first determined using the Hagen-Poiseuille laminar flow relationship between head loss and capillary diameter,

$$H_L = \frac{128\mu QL}{\rho g \pi D^4} \tag{7}$$

The head loss value was obtained from data collected between February and May of 2016 when 12-hour filtration runs with varying influent PACl concentrations reached filter failure in the lab scale filter. For the purpose of this study, analysis was done using the experimental parameters of a 12-hour filtration run with an influent PACl concentration of 0.65 $\frac{\text{mg Al}}{\text{L}}$, which resulted in a head loss of 62.7 cm and a failure time of 4.68 hours. Thus the diameter of the annulus formed at filter failure was calculated and used to determine the volume. The volume of the annulus at filter failure represented the volume of flocs retained in the filter at failure time. For the 0.65 $\frac{\text{mg Al}}{\text{L}}$ filtration run, the annulus inner diameter and volume were 151.4 μm and 0.023 cm^3, respectively.

A mass balance of clay and coagulant entering and exiting the filter was used to determine the mass of flocs retained in the filter. The mass of flocs accumulated in the filter after the 0.65 $\frac{\text{mg Al}}{\text{L}}$ filtration run was 0.091 mg, according to

$$m_{\text{FlocCap}} = (C_{\text{PACl}} Q_{\text{Cap}} + C_{\text{In}} Q_{\text{Cap}} - C_{\text{Out}} Q_{\text{Cap}}) t_{\text{failure}} \tag{8}$$

where m_{FlocCap} is the mass of flocs in one capillary tube, C_{PACl} is the concentration of PACl entering one capillary tube, Q_{Cap} is the flow of water into one capillary tube, C_{In} is the concentration of clay entering one capillary tube, C_{Out} is the concentration of clay exiting one capillary tube, and t_{failure} is the time until the filter failed. The density of the particles retained in the filter was then determined to be 994.85 $\frac{\text{kg}}{\text{m}^3}$ for the 0.65 $\frac{\text{mg Al}}{\text{L}}$ filtration run. However, when the buoyant density of flocs equation,

$$\rho_{\text{Floc}} = \rho_{\text{FlocInitial}} - \rho_{\text{H2O}}(T)\left(\frac{d_{\text{initial}}}{d}\right)^{3-D_{\text{Fractal}}} + \rho_{\text{H2O}}(T) \tag{9}$$

was utilized to calculate theoretical minimum and maximum floc densities, the empirical density was too low to be within a reasonable range. The variables in the equation were defined in the following way: ρ_{Floc} is the floc density, $\rho_{\text{FlocInitial}}$ is the primary particle density, $\rho_{\text{H2O}}(T)$ is the density of water at temperature T, d_{initial} is the initial floc diameter, d is the final floc

diameter, and D_{Fractal} is the fractal dimension of the floc. The temperature value corresponding to the 12-hour filtration run was 20°C, making the density of water at that temperature $992\frac{\text{kg}}{\text{m}^3}$. The fractal dimension was assumed to be 2.3 as predicted by the size ratio of colliding flocs in the filter *LL:* [Reference the journal section from Monroe's slides: Adachi Wat. Res. Vol. 31, No. 3, pp. 449 54, 1997. Also not sure why 2.3 is not sensitive to our calculations].

The minimum floc density calculation assumes that each floc has a diameter that is the largest it can be (the diameter of a pore), and the maximum floc density assumes that the floc diameter is the smallest it can be (the average diameter of kaolinite clay particles). The theoretical floc density range was determined to be 1037 $\frac{\text{kg}}{\text{m}^3}$ to 2128 $\frac{\text{kg}}{\text{m}^3}$. The calculated floc density of 994.85 $\frac{\text{kg}}{\text{m}^3}$ does not fall in this reasonable range. In addition, the floc diameter was determined by inputting the calculated empirical density into the buoyant density of flocs equation, Equation 9. The following table outlines the empirical and theoretical floc densities and diameters.

Table 1: Floc Diameters and Densities

Property	Empirical	Theoretical Min	Theoretical Max
Diameter (μm)	40370	4	408.25
Density ($\frac{\text{kg}}{\text{m}^3}$)	994.93	1037	2128

The capillary model can also be invalidated by analyzing the empirically-calculated floc diameter. While the capillary tube has a diameter of a pore, 0.41 mm, the empirical floc diameter was 42.3 mm, much larger than the diameter of a pore. Given these results, one single floc would not fit in the capillary tube, thus invalidating the capillary model. Moreover, an expected ratio of the volume of flocs to the volume of the pores was calculated by dividing the volume of flocs accumulated in a capillary tube at filter failure by the total volume of available pore space to be on the order of 10^{-3}. The calculated ratio of volume of flocs in a capillary tube to the volume of a clean capillary tube from the 0.65 $\frac{\text{mg Al}}{\text{L}}$ filtration run data was 0.862, which was much higher than the expected ratio. The analysis showed that flocs do not fill up majority of the pore volume, and the capillary model was abandoned.

The limitations of the capillary model informed the creation of a filter model of capillaries with constrictions to better depict the distribution of pore volume in the filter. Similar to the capillary model, the constriction model depicts the sand pores as capillaries with laminar flow from the top

to the bottom of one sand filter layer. However, the capillaries have a series of alternating constrictions and chambers.

Figure 4: This is a visual representation of the constriction model in one capillary tube. The sand grains are simply modeled as triangles on the outside, with water flowing between them. The constrictions are the where the tips of the triangles approach each other in the middle of the capillary.

The constrictions are openings between three tangent sand particles where the sand particles do not touch, whereas expansions consist of the entire volume enclosed between four tangent sand particles as seen in Figure 5.

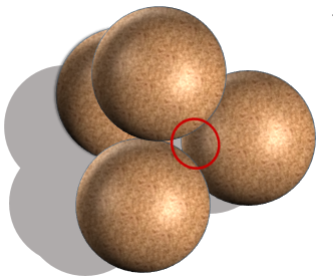

Figure 5: This is a visual representation of a constriction and an expansion. The openings created by tangent sand particles, as indicated by the red circle is a constriction. The volume enclosed within the four tangent sand particles is an expansion.

By assuming that each constriction has a height equal to the diameter of a sand particle, about 500 μm for the filter used in this study, it was approximated that there are 400 constrictions throughout one capillary tube, given the length of the filter.

During filtration, constrictions are hypothesized to be the primary locations on the sand grains to accumulate clay particles. The physical basis for the constriction model is that as streamlines converge at the constrictions, they collectively move closer to the constriction wall, allowing for more opportunities for clay particles to attach to the sand grain surfaces. In addition, when streamlines converge, particles carried along the streamlines have a greater chance of colliding with one another. It is hypothesized that the increase in collisions also contributes to clay particle accumulation on the walls of the constrictions. However, as the water continues past the constrictions, it expands in the chambers such that the streamlines move far apart from one another. The separation of the streamlines reduces the chance of collisions between the sand grain surfaces and the flocs in the water flowing through the expansions.

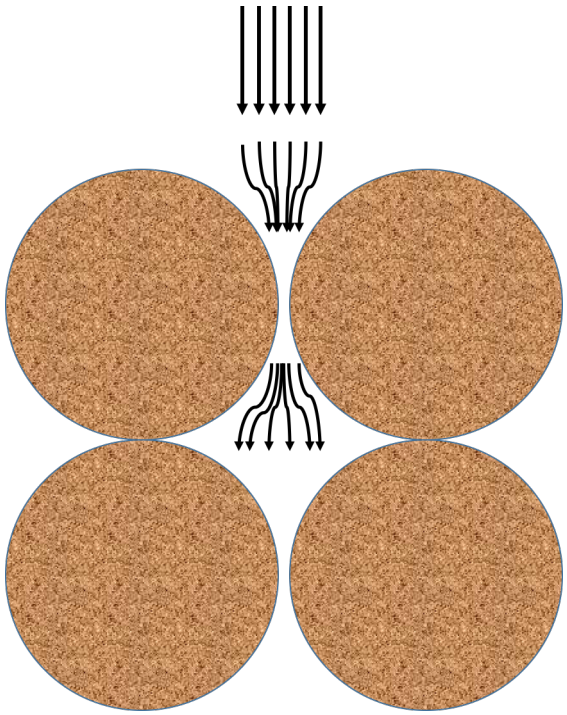

Figure 6: A depiction of streamlines passing through sand grains by converging and then expanding in a vertical cross sectional view of a constriction and expansion.

Following the converging streamline hypothesis, it was posited that there is a body of accumulated clay particles with a particular geometry at the constriction walls. Assuming the particles accumulated as a ring around the open pore with a vertical cross-sectional shape of a triangle, is the expected volume of particles captured. In modeling the floc mass as a rotated triangle, flocs accumulating at the constriction form a 45°angle with respect to the sand particle wall, Figures 7.

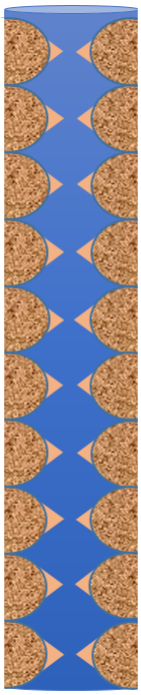

Figure 7: When looking at the vertical, cross-sectional area of one capillary tube at filter failure, the flocs accumulated at the constrictions are triangles.

When this volume was compared to the volume of pores, the ratio of captured particle volume to total pore volume was determined to be 0.125. However, through analysis of previously collected data, specifically failure head loss, failure time, and effluent turbidity, a ratio of captured particle volume to total pore volume was previously determined to be on the order of magnitude of 10^{-3}. The ratio calculated assuming particles accumulated as a triangular ring at each constriction was much larger than the expected ratio, a fault that invalidated the capillary model. In the capillary model, the ratio of capture particle volume to total pore volume was 0.862, much higher than the 0.125 determined in the constriction model. While there was significant improvement in decreasing the ratio to the expected 10^{-3} value, the constriction model depicted a much greater captured particle volume than the data suggested. Therefore, the volume of accumulated particles must be very small and it was speculated that the shape of the body of accumulated

flocs must be closer to that of a washer located at the constriction than a rotated triangle. In modeling the accumulated flocs mass as a washer, flocs effectively accumulate at a 0°angle with respect to the sand particle wall.

Washer Model

The low value for the expected ratio of captured particle volume to total pore space volume for the constriction model motivated the development of the washer model. The washer model is a really shallow, near zero angle version of the constriction model. A continuous capillary tube of pore space throughout the filter media with constrictions and expansions was still assumed in the model. However, to address the discrepancies of the constriction model, the washer model idealizes the build-up of flocs at each pore constriction as a washer of flocs in the constriction, as shown in Figure 8. The washer of flocs is hypothesized to have a very small volume to account for the low expected ratio of captured particle volume to total pore volume.

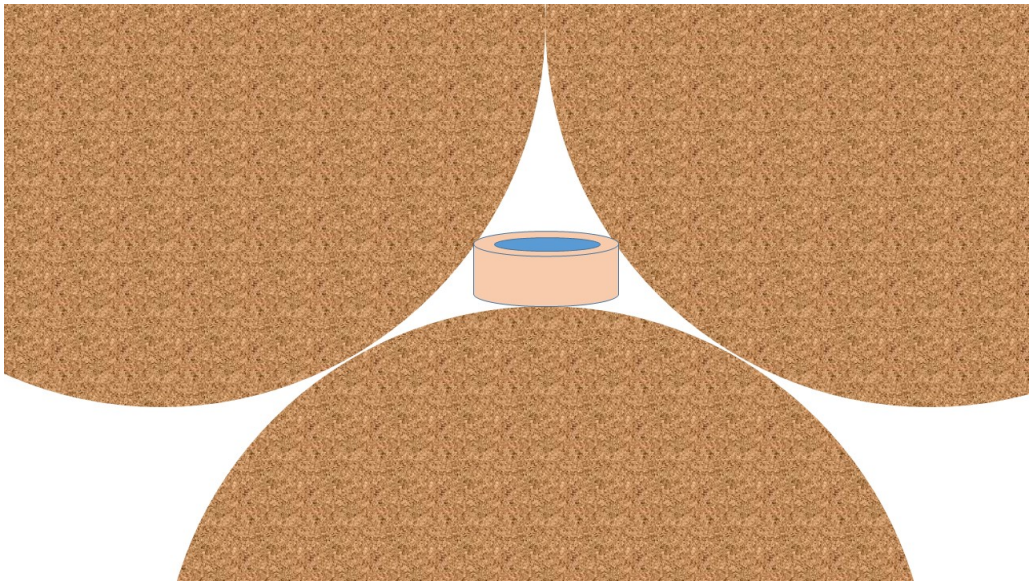

Figure 8: The proposed washer model has a layer of flocs coating the sand grain walls of the constriction, shown by the lighter-colored cylinder. Water flows through this washer of flocs in the blue region.

Head loss through the washer is hypothesized to be a minor loss due

to expansions and constrictions. The minor loss coefficient is based on the ratio between the diameter of the capillary and diameter of the constriction. Based on the measured head loss, the diameter of the clogged constriction (or the inner diameter of the washer) could be calculated with the following relationship

$$H_L = \left(\frac{D^2_{\text{Capillary}}}{\Pi_{\text{VC}} D^2_{\text{Constriction}} - 1} \right) \frac{V^2_{\text{Capillary}}}{2g} \tag{10}$$

Equation 10 for minor loss where $D_{\text{Capillary}}$ is the diameter of the capillary, 408 μm; $D_{\text{Constriction}}$ is the diameter of the constriction, 77.3 μm; $V_{\text{Capillary}}$ is the velocity of water through a capillary tube, 4.6 $\frac{\text{mm}}{\text{s}}$; and Π_{VC} is the vena contracta coefficient, 1. Π_{VC} represents the ration between the contracted area and the area of the orifice. The vena contracta coefficient was assumed to be one because it was hypothesized that there is a gradual decrease in area from the expansion to the constriction.

Future flocs would then attach to this washer of flocs instead of the sand grains. The following relationship between the dimensions of a washer of flocs and the capillary tube can be used to find the height of the floc build-up in the constriction:

$$\frac{H_{\text{Washer}} A_{\text{Washer}}}{H_{\text{Capillary}} A_{\text{Capillary}}} = \frac{V_{\text{Flocs}}}{V_{\text{Capillary}}}. \tag{11}$$

where H_{Washer} is the height of the floc build-up, A_{Washer} is the cross sectional area of the washer, $H_{\text{Capillary}}$ is the height of the capillary, $A_{\text{Capillary}}$ is the area of the capillary, V_{Flocs} is the volume of flocs, and $V_{\text{Capillary}}$ is the volume of a capillary.

While the constriction model may explain the process of particle collision and attachment at each constriction, the model simplifies the filter pores as straight capillaries from the top of the filter to the bottom. In reality, water does not flow straight through a single capillary. Instead, water weaves through the pores, affecting how particles mix within the filter. Thus, the washer model must be altered to account for the realistic water flow.

Experimental Protocols

Experimental Apparatus and Chemicals

A stacked rapid sand filter was created at the laboratory scale using a column of clear PVC pipe filled with sand. A schematic of the apparatus can be seen in Figure 1. The PVC pipe had an inner diameter of 2.6 cm and was 65 cm high. Sand sieved from sieve numbers 30 to 35 (0.595 mm to 0.500 mm) was used as the filter media and filled the column to a height of 40 cm. The porosity of the sand was assumed to be 0.4 ([INSERT REFERENCE]). The approach velocity in the filter was 1.8 mm/s and the overall flow rate of the system was 1.98 mL/s. Correspondingly, the residence time of the filter was 43.6 s.

The inlet and outlet pipes were made of copper pipe with an inner diameter of 9.4 mm. The inlet pipe was a replica of an injection system that was made of PVC pipe with closely spaced downward-facing holes. The original injection system was made up of PVC pipe with an outer diameter of 3.34 cm (nominal diameter 1") and a 10 cm center-to-center distance between orifices for sand layers that were 20 cm deep. The ratio of the areas of the orifice and filter is equivalent to the ratio of the inlet pipe outer diameter to the spacing between orifices, described by

$$\frac{A_{\mathrm{Or}}}{A_{\mathrm{Fi}}} = \frac{OD_{\mathrm{Pipe}}}{B_{\mathrm{Or}}}. \tag{12}$$

The resulting area of the orifice for the laboratory filter was 1.8 cm^2. To maintain this area for the inlet pipe with insufficient surface area for a circular orifice, a rectangular orifice of the inlet pipe was cut with dimensions of 0.80 cm x 2.24 cm. Copper mesh with openings of 0.23 x 0.23 mm and a porosity of 0.3 was welded to the outlet pipes of the filter to prevent unintended media removal.

The coiled tube flocculator was made of clear flexible tubing with an inner diameter of 0.625 mm and a length of 1.32 m. The flocculator was designed with a residence time of 2.67 s for a flow rate of 1.98 mL/s. The energy dissipation rate was 0.27 W/kg, which kept flocs small to simulate influent water for filtration.

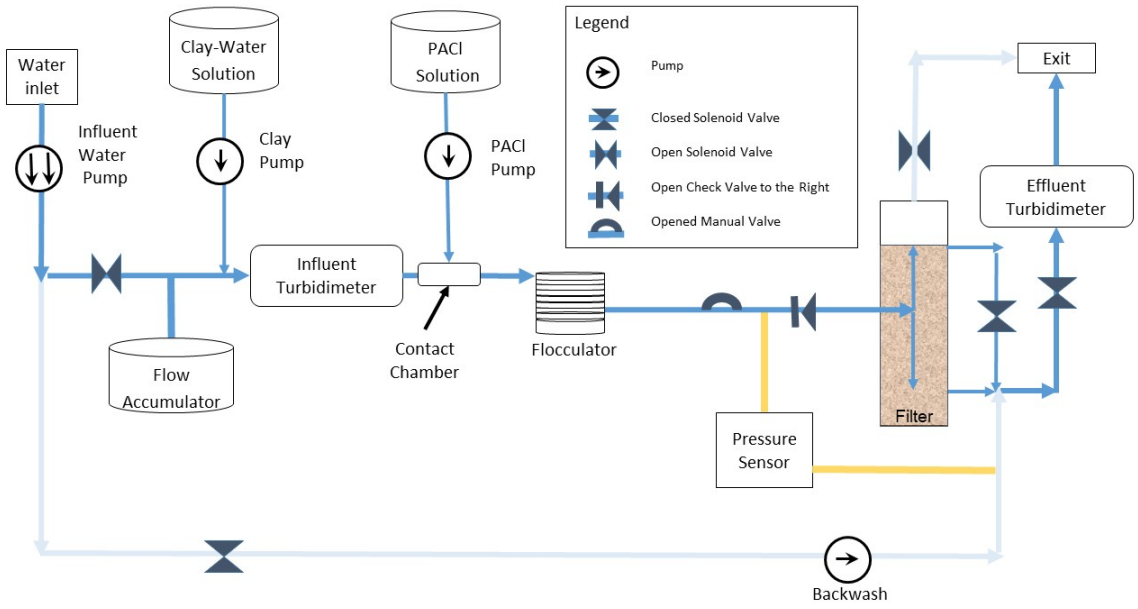

Figure 9: Schematic for the experimental filter apparatus in filter mode showing influent and effluent turbidimeter sampling systems, PACl solution and clay, humic acid solution dosing, pressure sensor to measure filter head loss, and flocculator. Blue connections are used in filter mode. Gray connections are used in backwash mode.

Tap water was pumped through the experimental apparatus from a connection to the tap water source using a 600 RPM peristaltic pump (Masterflex model 7519-15). The tap water at Cornell University has an average turbidity of 0.057 NTU, a total hardness of 150 mg/L, a total alkalinity of 108 mg/L, a pH of 7.44, a dissolved organic carbon concentration of 1.95 mg/L, a pH of 7.36, and a water hardness of approximately 150 $\frac{\text{mg}}{\text{L}}$ Bolton Point et al. (2016).

As the water flowed through the apparatus, a clay and humic acid-water solution was pumped into the influent water using a 100 RPM peristaltic pump (Masterflex model 7518-00) to imitate a raw water solution of 5 NTU. Turbid raw water was simulated with a 0.836 $\frac{\text{g}}{\text{L}}$ suspension of kaolinite clay (R.T. Vanderbilt Co., Inc., Norwalk, Connecticut). To simulate natural organic matter, humic acid (Sigma-Aldrich Corp., St. Louis, MO) was also

added to the solution at 0.098 $\frac{\text{g}}{\text{L}}$ so that a concentration of 1 $\frac{\text{mg}}{\text{L}}$ of humic acid was maintained in the system. A PID control system monitoring influent turbidity measurements ensured that the influent water remained at 5 NTU throughout the filtration process.

Polyaluminum chloride, or PACl (Holland Company, Adams, MA), was used as the coagulant with concentrations of 100 $\frac{\text{mg Al}}{\text{L}}$ and 150 $\frac{\text{mg Al}}{\text{L}}$. A 100 RPM peristaltic pump (Masterflex model 7518-00) transferred PACl solution into a contact chamber to mix with the influent water.

From the contact chamber, the influent flowed through a coiled-tube flocculator, where PACl coagulated clay and coagulant nanoclusters. The flocculated water entered the filter through the inlet pipe, with the flow splitting above and below the filter media. Effluent water exited through two outlet pipes, which then merged before entering the effluent turbidimeter.

During the backwash process for cleaning the filter media, water was pumped into the filter from the bottom of the filter, and it flowed to the top of filter column. The upflow backwash velocity was 11 mm/s. The increased velocity expanded the sand bed such that particles trapped in the sand pores detached from the particles and effectively removed flocs from the sand particles.

Data Collection and Analytical Methods

Influent and effluent turbidities were measured with two turbidimeters (HF Scientific MicroTOL). Head loss across the filter was measured with a differential pressure sensor connected to the tubing before the filter inlet tube and after the confluence of the two tubes exiting the filter. Data was collected every 5 s but was smoothed for 30 s intervals to reduce noise.

Filtration performance was measured by pC^*, which is the negative log of the ratio of effluent turbidity to influent turbidity:

$$\text{p}C^* = -\log_{10} \frac{\text{EffluentTurbidity}}{\text{InfluentTurbidity}}. \tag{13}$$

Filter failure may be chosen as the time when breakthrough occurred in the filter, which is when the rate of change of pC^* was the most negative and the effluent turbidity was increasing most rapidly from previous values. Another measure of filter failure time was when the head loss reached the maximum allowable head loss before breakthrough, which has been empirically found to be at least 60 cm. Generally, whichever threshold was reached

first determined filter failure time. For these analyses, the time of breakthrough was used as the failure time.

Results

Filter Performance

Head loss data from the lab-scale filter experiments demonstrate a linear increase in head loss until filter failure time, as seen in Figure 1, regardless of the concentration of PACl entering the system. However, after filter failure, head loss increase appears to slow down. Figure 1 suggests that if the filter run time were longer, there is a possibility of the head loss approaching a maximum value.

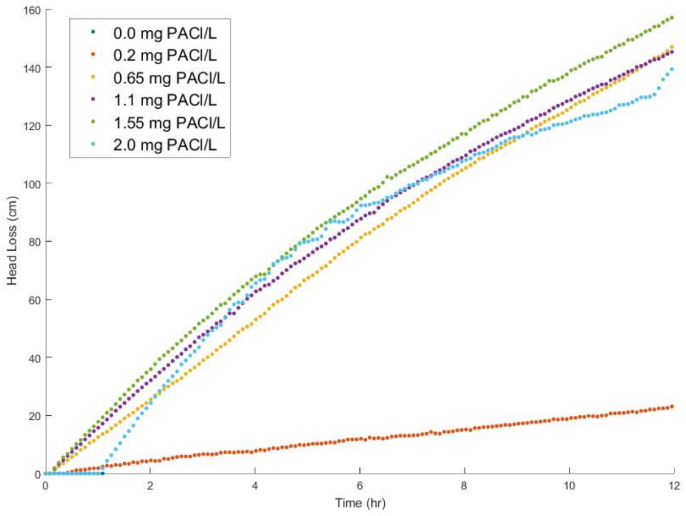

Figure 10: Head loss increases linearly until filter failure. Influent turbidity was 5 NTU and the flow rate through each layer is 0.984 mL/s.

When effluent turbidity data were analyzed, it was clear that while effluent turbidity was relatively constant, there was a very slight increase in performance during the filter run as indicated by the slight negative slope on Figure 11. LL: [These graphs were made in Matlab and will require some extra time to adjust the scale to look at the effluent turbidity before filter failure.] While

there was no trend in the relationship between effluent turbidity and PACl dosage, there was a consistent increase in performance in filtration in each experiment leading up to the time of failure. This suggests that there is a mechanism of particle removal through the filter allowing for cleaner water right before filter failure.

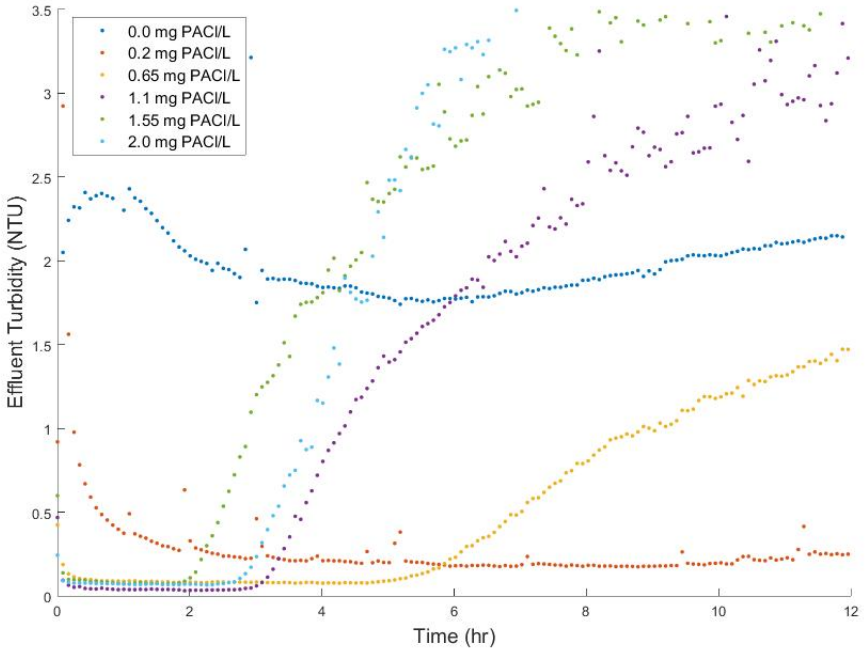

Figure 11: The filter fails when effluent turbidity increases at a rapid rate (steep slope). Influent turbidity is 5 NTU and the flow rate through each filter layer is 0.98 mL/s.

LL: [Reference and code to insert a figure is already here; just need to upload the new graph and change the name of the figure in comments below.]

Inconsistent Filter Performance

Experiments conducted to clog the filter showed that the same influent water conditions resulted in varying performance levels and failure times. When the influent water was 5 NTU and the PACl dosage was 2 mg/L, as shown

in Figures 12 and 13, failure times ranged from 1.6 hours to 3 hours. Filter performance also varied, where one experiment did particularly well at an average effluent turbidity of 0.07 NTU and a pC^* of over 1.8, but this performance was not achieved in other experiments

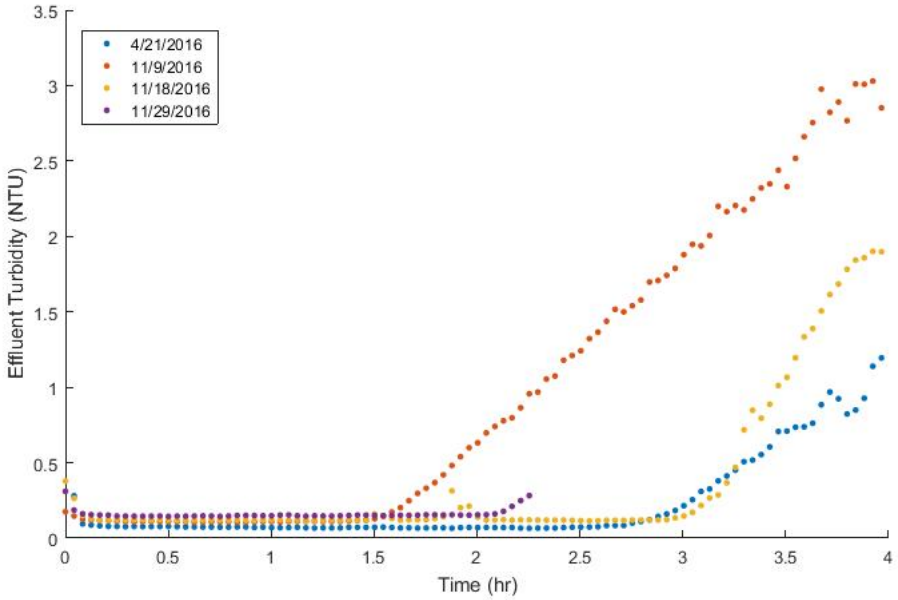

Figure 12: Effluent turbidity for experiments where influent turbidity was 5 NTU and PACl dosage was 2 mg/L.

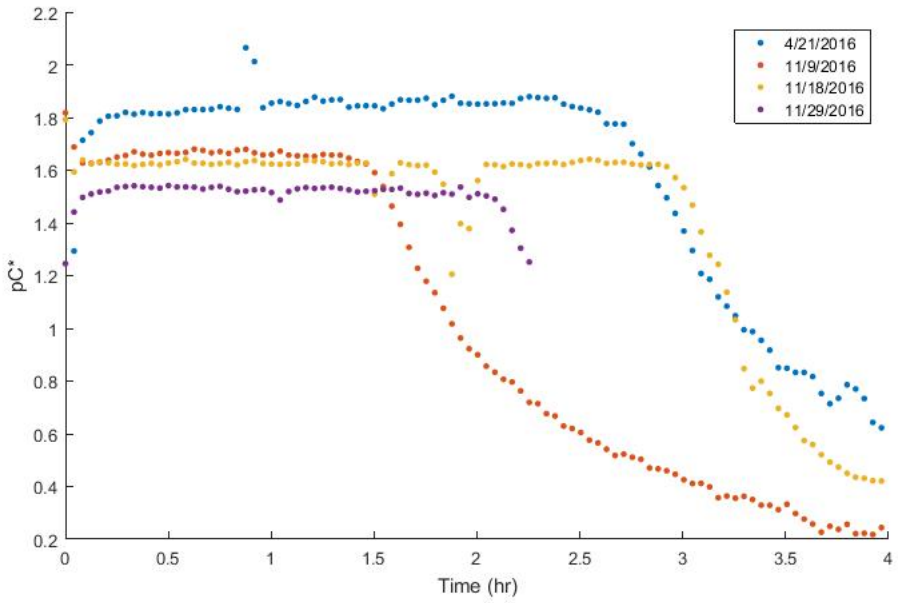

Figure 13: p$C*$ where influent turbidity was 5 NTU and PACl dosage was 2 mg/L.

Clean Bed Head Loss

A preliminary experiment was conducted to determine the relationship between head loss and velocity through the lab-scale filter. In assessing the behavior of head loss at various flow rates, it is possible to determine the dominant mode of head loss during filtration, and thus find a more realistic model of filter performance. To perform this assessment, head loss was recorded while the flow rate though a clean lab scale filter was varied. The data demonstrated that head loss varied linearly with velocity as suggested by the trend line on Figure 14. This implied that the flow through a clean sand bed is dominated by major head losses, as described by the Carmen-Kozeny equation, Equation 14 (Benjamin and Lawler, 2013).

$$h_{\text{Major}} = 36 H_{\text{FiSand}} k \frac{1-\phi_{\text{FiSand}}}{\phi^3_{\text{FiSand}}} \frac{\nu V_{\text{Fi}}}{g D^2_{60}} \tag{14}$$

where h_{Major} is the major head loss, ϕ_{FiSand} is the porosity of the sand, H_{FiSand} is the height of the sand bed, and D_{60} is the diameter at which 60% of the

particles in the sand bed will be removed by a series sieves.

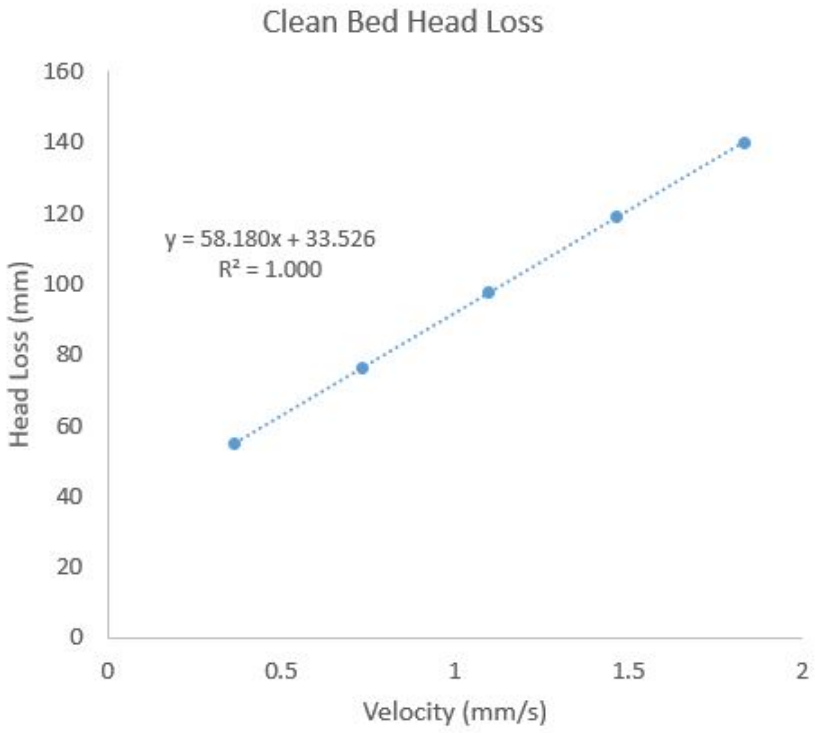

Figure 14: The head loss in a clean bed filter has a linear relationship with velocity. This relationship indicates that major losses are the only significant contributing factor.

Dirty Bed Head Loss

To understand the head loss behavior of a filter containing removed particles, an experiment was conducted to clog the filter and record head loss values as flow rate was decremented. The data suggested that head loss in a dirty sand bed was influenced by major and minor losses, as the best-fit trend line was a quadratic equation. The coefficient of the linear term indicated major losses and the coefficient of the square term indicated the minor losses, shown in Equations 14 and 15, respectively. The quadratic relationship between head loss and velocity suggested that minor losses are significant in a dirty sand bed, with a minor loss coefficient as large as 4954. The coefficient was

calculated using the minor loss equation,

$$h_{Minor} = \frac{KV_{Fi}^2}{2g} \tag{15}$$

where K is the minor loss coefficient, V_{Fi} is the velocity through the filter, and h_{Minor} is the minor head loss as shown in the following figure.

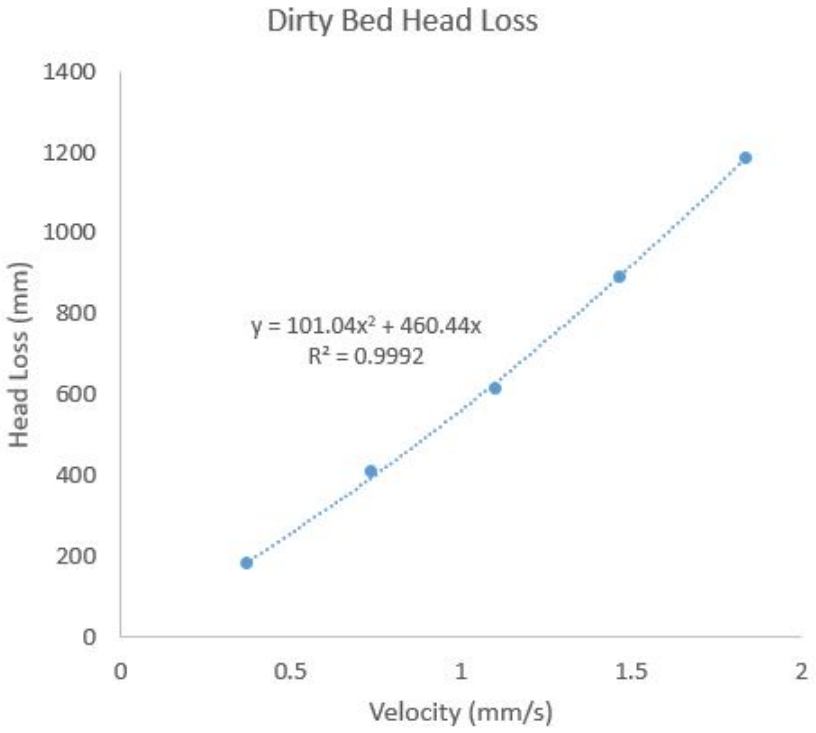

Figure 15: The head loss in the filter for a clogged filter has a quadratic relationship with velocity, indicating that minor losses are significant.

Effect of Flow Rate on Particle Capture

One hypothesis tested was that lowering the flow rate after initial clogging would allow for greater particle capture. An experiment tested the effect of flow rate in the filter by running the system at the full flow rate of 0.98 mL/s for one hour and then at 0.49 mL/s for 24 hours. The effluent turbidity was expected to drop soon after lowering the flow rate. According to Figure 16 below, the turbidity did not change with the drop in flow rate.

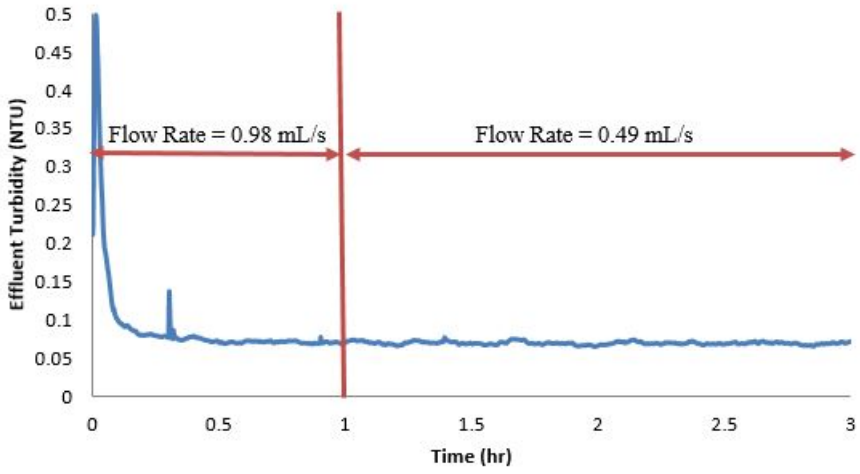

Figure 16: The flow rate was lowered after one hour. Effluent turbidity did not change with a change in flow rate.

Discussion

Active Zone Hypothesis

It was hypothesized that flocs accumulate as a single mass in one concentrated region until the region can no longer retain particles. To better describe the process, the flocs build up such that the effective diameter of the region decreases until the shear force due to the water flowing through the region becomes too high for particle attachment, at which point the region has the minimum effective diameter and ceases to retain particles. When the region reaches maximum particle retention ability, the region becomes part of the dirty bed and particle accumulation occurs in empty pore volume further downstream in the filter. This process continues until the wall of the capillary tube running along the length of the sand column is filled with flocs and the sand bed effectively becomes a dirty bed. *WP:* Despite mixing and particle movement in the sand bed during filtration, the head loss during filtration did not correlate with the expected random motion. [I'm not exactly sure what you mean by this. If you look at the Darcy-Weisbach equation, the velocity term is always squared whether the flow is laminar (ordered) or turbulent (random); what changes is the way the friction factor, a coefficient, is calculated. I might be missing

something, but it seems that you need to express the physical argument in a different way.] Instead, the linear increase in head loss suggests that there is uniform clogging of the pores in the filter as the active zone moves down the filter. The observed constant change in head loss further suggests that the pores at the forefront of the active zone are all removing particles at a constant rate. However, following the active zone hypothesis, the active zone moved through the filter resulting in an increase in dirty bed depth and a decrease in clean bed depth during filtration. It was assumed that the only variables changing during the process were the dirty and clean bed depths, suggesting that as dirty bed depth increased, there would also an increase in filter performance. However, at some point the filter failed with a very narrow filter failure period as indicated by the steep slope of effluent turbidity in figure 11. The narrow filter failure period demonstrated that, when the active zone reached the end of the filter bed, filter performance decreased drastically. At failure, the entire sand bed was filled with particles and there was no active zone. Without an active zone, most particles exited the filter as there were no opportunities to attach to the sand grains.

Sand Bed Head Loss

The results shown in Figure 15 showed that higher velocities resulted in higher rates of head loss accumulation and that minor losses are present, which exist due to expansions and contractions in flow. The washer model of filter media constrictions is supported by these observations since these proposed changes in flow areas can be significant contributors to head loss, as modeled.

Maximizing Filter Effectiveness

Particle capture occurs through the mechanism of interception, where particles collide with the filter media along their paths of travel. When a sand bed is already filled with particles, the already-captured particles would serve as an extension to the filter media and allow for improved capture of smaller particles. Moreover, reducing the flow rate reduces the shear through the sand pores. Hence, smaller particles entering the filter would not remain in suspension; instead they will follow the fluid shearing through the sand pores and attach to the already-captured particles accumulated at the filter media surface. However, when flow rate was reduced after clogging the lab scale

filter, results show that there is no change in effluent turbidity, Figure 16. This suggests that the limiting factor in filter effectiveness is not in particle size. Regardless of particle size in suspension, the smaller particles that were expected to be captured at a lower flow rate, thus a lower shear were not. Instead, a new hypothesis is that particles that continue to pass through to the effluent water may not have had enough coagulant, since the results shown in Figure 16 indicate that it is a property of the particles, rather than the flow, that keeps them from being intercepted.

Summaries

Acknowledgments

Disclosure

None of the authors of this paper have any competing financial interests.

Corresponding Author

(Name)
Phone:
E-mail:

References

Adelman, M. J., Weber-Shirk, M. L., Cordero, A. N., Coffey, S. L., Maher, W. J., Guelig, D., Will, J. C., Stodter, S. C., Hurst, M. W., and Lion, L. W. (2012). Stacked Filters: Novel Approach to Rapid Sand Filtration. *Journal of Environmental Engineering*, 138(10):999–1008.

Benjamin, M. and Lawler, D. (2013). *Water quality engineering: physical / chemical treatment processes*. Wiley, Hoboken, N.J.

Bolton Point, City of Ithaca, and Cornell University (2016). Annual Drinking Water Quality Report | Ithaca, NY - Official Website.

Iwasaki, T., Slade, J. J., and Stanley, W. E. (1937). SOME NOTES ON SAND FILTRATION [with Discussion]. *Journal (American Water Works Association)*, 29(10):1591–1602.

Jegatheesan, V. and Vigneswaran, S. (2003). Mathematical modelling of deep bed filtration. volume 4, pages 1805–1810, Townsville, QLD, Australia. Modelling & Simulation Society of Australia & New Zealand.

Rajagopalan, R. and Tien, C. (1976). Trajectory analysis of deep-bed filtration with the sphere-in-cell porous media model. *AIChE J.*, 22(3):523–533.

Rajagopalan, R. and Tien, C. (1977). Single collector analysis of collection mechanisms in water filtration. *Can. J. Chem. Eng.*, 55(3):246–255.

Zamani, A. and Maini, B. (2009). Flow of dispersed particles through porous media — Deep bed filtration. *Journal of Petroleum Science and Engineering*, 69(1–2):71–88.

Zhi, H. (2016). Arsenic(V) Removal From Drinking Water By Concurrent Introduction Of As Contaminated Water And Polyaluminum Chloride In A Sand Filter Medium.